



Consequences of rapid ice sheet melting on the Sahelian population vulnerability

Dimitri Defrance^{a,b,1}, Gilles Ramstein^a, Sylvie Charbit^a, Mathieu Vrac^a, Adjoua Moïse Famien^{b,c}, Benjamin Sultan^b, Didier Swingedouw^d, Christophe Dumas^a, François Gemenne^{e,f}, Jorge Alvarez-Solas^g, and Jean-Paul Vanderlinden^e

^aLaboratoire des Sciences du Climat et de l'Environnement, Institut Pierre Simon Laplace, Commissariat à l'Énergie Atomique et aux Énergies Alternatives - CNRS - Université de Saint-Quentin-en-Yvelines, Université Paris-Saclay, 91141 Gif-Sur-Yvette, France; ^bUniversité Pierre et Marie Curie - CNRS - Institut de Recherche pour le Développement - Muséum National d'Histoire Naturelle, Laboratoire d'Océanographie et du Climat: Expérimentations et Approches Numériques, Institut Pierre Simon Laplace, 75005 Paris, France; ^cLaboratoire de Physique de l'Atmosphère, Université Félix Houphouët Boigny, 22 BP 582 Abidjan, Côte-d'Ivoire; ^dEnvironnements et Paléoenvironnements Océaniques et Continentaux, CNRS, Université de Bordeaux, 33615 Pessac, France; ^eCultures Environnements Arctique Représentations Climat, Observatoire de Saint-Quentin-En-Yvelines, Université Paris-Saclay, 78280 Guyancourt, France; ^fThe Hugo Observatory, Fonds de la Recherche Scientifique, University of Liège, 4000 Liège, Belgium; and ^gPalMA Group, Universidad Complutense de Madrid, 28040 Madrid, Spain

Edited by Anders Levermann, Potsdam Institute for Climate Impact Research, Potsdam, Germany, and accepted by Editorial Board Member Hans J. Schellnhuber May 11, 2017 (received for review December 3, 2016)

The acceleration of ice sheet melting has been observed over the last few decades. Recent observations and modeling studies have suggested that the ice sheet contribution to future sea level rise could have been underestimated in the latest Intergovernmental Panel on Climate Change report. The ensuing freshwater discharge coming from ice sheets could have significant impacts on global climate, and especially on the vulnerable tropical areas. During the last glacial/deglacial period, megadrought episodes were observed in the Sahel region at the time of massive iceberg surges, leading to large freshwater discharges. In the future, such episodes have the potential to induce a drastic destabilization of the Sahelian agroecosystem. Using a climate modeling approach, we investigate this issue by superimposing on the Representative Concentration Pathways 8.5 (RCP8.5) baseline experiment a Greenland flash melting scenario corresponding to an additional sea level rise ranging from 0.5 m to 3 m. Our model response to freshwater discharge coming from Greenland melting reveals a significant decrease of the West African monsoon rainfall, leading to changes in agricultural practices. Combined with a strong population increase, described by different demography projections, important human migration flows could be potentially induced. We estimate that, without any adaptation measures, tens to hundreds million people could be forced to leave the Sahel by the end of this century. On top of this quantification, the sea level rise impact over coastal areas has to be superimposed, implying that the Sahel population could be strongly at threat in case of rapid Greenland melting.

climate change | ice sheet melting | impact | vulnerability | Sahel

The Sahel is particularly exposed to extreme climate variability, as evidenced by the impacts of the severe droughts in the late 20th century (1). Paleoclimatic records have also shown that megadrought episodes occurred in this area during past glacial/deglacial periods (2–5) at the time of huge surges of icebergs (i.e., the so-called Heinrich events), causing outlet glacier acceleration and thus sea level rise (6, 7) (SLR). Several modeling studies performing water-hosing experiments confirmed the close correspondence between the West African monsoon weakening and the freshwater flux (FWF) released to the ocean (8–10) due to ice sheet melting. These studies raise the question as to whether such episodes could occur during this century in response to a massive freshwater discharge triggered by a significant ice sheet destabilization or surface melting and, if so, what would be the related environmental and human impacts in the Sahel area.

According to the latest Intergovernmental Panel on Climate Change Fifth Assessment Report (AR5) (11), the likely range of global mean SLR under the Representative Concentration Pathways 8.5 (RCP8.5) scenario is 0.52 m to 0.98 m by the end of the 21st century. Although considerable progress has been made in ice

sheet modeling over the last decade, this range is provided with only medium confidence, due to large remaining uncertainties in the ice sheet dynamic response and to an improper representation of the ice–ocean interactions (12).

In Greenland, recent observations of fjords standing well below sea level suggest important processes of glacier front destabilization (13) that are not included in the current dynamic ice sheet models (14). Moreover, although there are only a few ice shelves surrounding Greenland compared with West Antarctica, post-AR5 remote sensing observations reveal that ice shelves have experienced a continuous thinning for several years, resulting in a buttressing weakening (15, 16), not only in the Antarctic ice sheet but also in Greenland. This leads to a significant ice stream acceleration and possibly to a massive discharge of grounded ice, similar to what occurred during Heinrich events or, more recently, after the collapse of the Larsen B ice shelf (17). Moreover, past episodes of rapid SLR acceleration, such as the Meltwater Pulse 1A (18), are still raising questions about our ability to evaluate the future SLR under current understanding of physical mechanisms.

Results from these past climate studies combined with present-day observations suggest that the ice sheet contribution to SLR could have been underestimated. Here, we consider different freshwater discharge scenarios equivalent to an additional SLR ranging from 0.5 m to 3 m coming from ice sheet melting and/or destabilization,

Significance

A major uncertainty concerning the 21st century climate is the ice sheet response to global warming. Paleodata indicate rapid ice sheet destabilizations during the last deglaciation, which could lead to an underestimation of sea level rise, as suggested in recent publications. Therefore, we explore the impact of different scenarios of Greenland partial melting in the very sensitive Sahel region. We first demonstrate that such a melting induces a drastic decrease of West African monsoon precipitation. Moreover, we quantify the agricultural area losses due to monsoon changes. Consequently, we pinpoint a large potential for migration of millions of people in the coming decades. Thus, the ice sheet destabilization provokes not only coastal damages but also large population migration in monsoon area.

Author contributions: D.D., G.R., B.S., D.S., and C.D. designed research; D.D. and C.D. performed research; M.V. and A.M.F. contributed new reagents/analytic tools; D.D., S.C., A.M.F., D.S., F.G., J.A.-S., and J.-P.V. analyzed data; and D.D., G.R., and S.C. wrote the paper.

The authors declare no conflict of interest.

This article is a PNAS Direct Submission. A.L. is a guest editor invited by the Editorial Board.

¹To whom correspondence should be addressed. Email: dimitri.defrance@ird.fr.

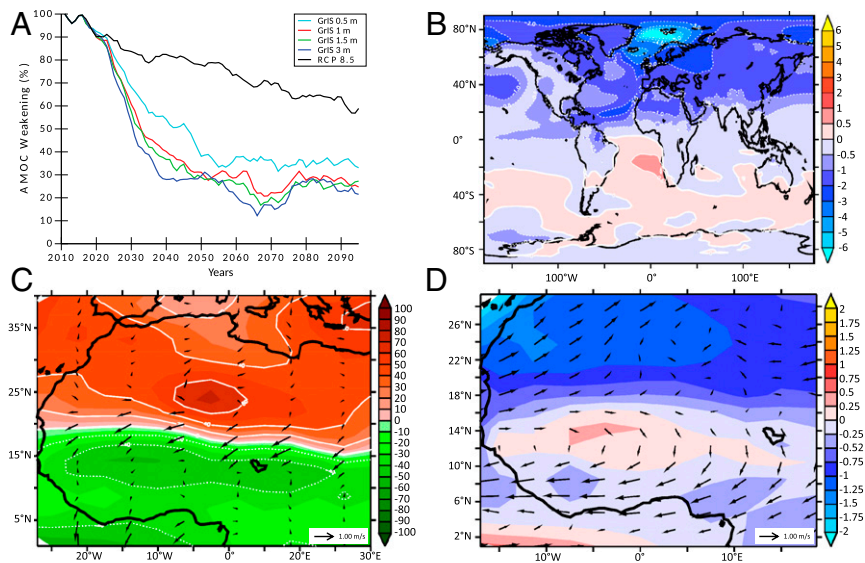


Fig. 1. Teleconnection mechanisms linking the Greenland ice sheet melting and the decrease of the Sahelian rainfall. (A) AMOC evolution (in percent with respect to the present-day values). (B) Mean annual temperature anomaly between the 1.5-m GrIS and the RCP8.5 scenarios averaged over the period 2030–2060. (C) Same as B but for the sea level pressure anomaly, and the 10-m winds (black arrows). (D) Same as B but for the mean summer (JJAS) temperature anomaly and the 850-hPa winds (black arrows).

which is not accounted for in the baseline RCP8.5 climate simulation. We explore the related climatic effects on the West African monsoon over the 21st century and their ensuing impacts on the Sahelian cultivable areas and thus on the local population.

Using the Institut Pierre Simon Laplace low resolution coupled ocean–atmosphere model (IPSL-CM5A-LR) [same version as in the Coupled Model Intercomparison Project, Phase 5 (CMIP5) exercise (19); *Methods*] run under the RCP8.5 radiative forcing from 2006 to 2100, we performed four different water-hosing experiments superimposed to the RCP8.5 scenario in which we added, respectively, a 0.11-, 0.22-, 0.34-, and 0.68-Sv FWF ($1 \text{ Sv} = 10^6 \text{ m}^3 \cdot \text{s}^{-1}$) released in the North Atlantic from 2020 to 2070 and corresponding, respectively, to 0.5-, 1-, 1.5-, and 3-m SLR. Our goal is, first, to investigate the climatic impacts of the FWF coming from Greenland (GrIS scenarios) in the West African region and, second, to show the impacts on the cereal cultivation in the Sahel area, and the consequences for the local population, which is already facing chronic malnutrition problems.

Changes in Tropical Precipitation Systems

It has been shown that the freshening of the North Atlantic has global climatic impacts (9, 20–25), including a strong cooling of the Northern Hemisphere down to the Sahara (26–29) related to a very strong slowdown of the North Atlantic Deep Water (NADW) leading to the slowdown of the Atlantic meridional overturning circulation (AMOC) (9, 20–24). The maximum decrease of the mean annual NADW outflow at 30°N occurs around 2060 and corresponds to a reduction of 90% (60%) of the initial NADW value associated with a sea level rise of 3 m (0.5 m) (Fig. 1A). This feature is associated with a large decrease of Sahel rainfall (10% to 60%) between 2030 and 2060 with respect to the RCP8.5 scenario (Fig. 2). This spatial pattern of precipitation changes is similar to the one inferred from the large surge of iceberg discharges that occurred in the past (2, 30). The tropical rainfall changes are linked to the Northern Hemisphere cooling through atmospheric teleconnections. A north–south thermal gradient between the Sahara (cooler) and the Guinea Gulf (warmer) appears (Fig. 1B). This gradient leads to a rise of sea level pressure gradient, inducing low-level southward winds, which block the monsoon system farther south (Fig. 1C). The Sahel becomes drier, and the surface

temperature increases; this causes an additional local temperature gradient that strengthens the African Easterly Jet, causing a moisture export from this area (2, 31) (Fig. 1D). These mechanisms underlying the drastic reduction of Sahelian precipitation are robust in different climatic contexts with several models (9, 22).

Here we focus on the Western African Sahel region (8°N to 18°N; 17°W to 15°E). Because the Sahelian population is strongly dependent on pastoralism and rainfed agriculture for subsistence (32), our analysis is made in terms of summer precipitation changes [June to September (JJAS)] during which most of the rainfall occurs (between 80% and 90%). To circumvent the acknowledged difficulties of CMIP5 models (33) to properly capture the mesoscale processes and therefore the monsoon rainfall, we applied a statistical method to improve the IPSL simulated precipitation in the West African region with respect to the Water and Global Change project (WATCH) Forcing Data methodology applied to the latest global atmospheric reanalysis data produced by the European Centre for Medium-Range Weather Forecasts (ERA-Interim) (WFDEI) reanalysis (34). This method, called “Cumulative Distribution Function transform” (CDF-t), has been successfully applied in many climate-related studies (e.g., refs. 35–38; *Methods*).

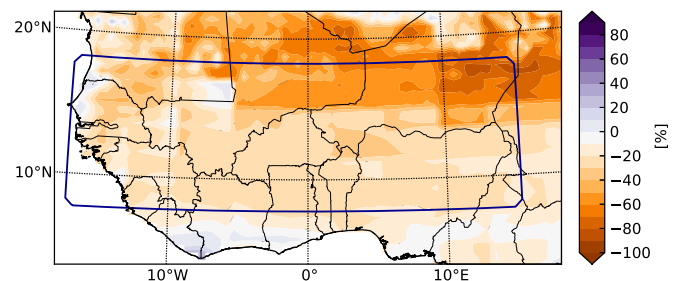


Fig. 2. JJAS precipitation anomaly between the 1.5-m GrIS scenario and the RCP8.5 baseline experiment normalized to the RCP8.5 values and averaged over 2030–2060. A value of 100 corresponds to a doubling of precipitation, and -100 corresponds to zero precipitation. The precipitation values are obtained after applying the statistical method (*Methods*). The blue box (8°N to 18°N, 17°W to 15°E) represents the region under study.

To illustrate the internal model variability, we considered a four-member dataset of the RCP8.5 scenario, each member differing in initial conditions. The evolution of the corrected precipitation in the West African Sahel region, obtained under the RCP8.5 dataset (baseline experiments) and the four GrIS scenarios, is displayed in Fig. 3. However, the precipitation signal simulated in response to the 0.5-m SLR perturbation is not statistically significant compared with the four members of the RCP8.5 baseline experiment, as indicated by the t test (P value <0.05 ; *Methods*), and the corresponding results will not be further discussed in the following.

The effect of the FWF perturbation radically changes the evolution of precipitation averaged over the Sahel region. The first key feature is a significant decrease of Sahel rainfall for the three larger GrIS scenarios (i.e., 1-, 1.5-, and 3-m equivalent SLR) compared with the four-member RCP8.5 dataset. This decrease occurs almost concomitantly with the FWF release and can be up to 30% over the period 2030–2060, reaching $3 \text{ mm}\cdot\text{d}^{-1}$, where the greatest differences with the baseline experiment scenario are simulated (P value <0.05). When the freshwater perturbation stops, Pav increases slightly, and values close to those of the baseline experiment are recovered.

Increasing Vulnerability

The Sahelian agroecosystem is likely to be strongly disturbed by these large precipitation changes; this could have significant impacts on populations extremely dependent upon rainfed agriculture for subsistence. It is documented that the rainfall decrease and the temperature elevation in the Sahel will negatively impact yields of staple food cereals, such as sorghum and millet (39). The water demand for these crops is calculated by Food and Agriculture Organization (FAO) formulations (*Methods*) and depends on temperature. The north–south gradient of water demand has a similar amplitude for sorghum and millet, directly related to the temperature gradient. In the Sahel area, the sorghum needs, currently, between 520 mm and 660 mm per growing period. The millet growth period is shorter than that of sorghum and needs therefore less water (460 mm to 600 mm per growing period). The

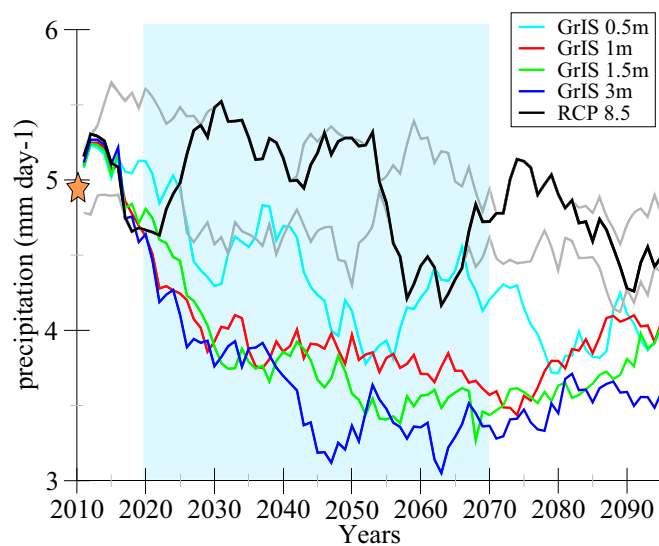


Fig. 3. Evolution of JJAS precipitation during the 21st century averaged over the Sahel area (8°N to 18°N , 17°W to 15°E) for the RCP8.5 and the GrIS scenarios. The orange star indicates the simulated JJAS precipitation over the climatic reference period (1976–2005) deduced from the IPSL-CM5A simulated precipitation (4.96 mm). To illustrate the internal model variability, we considered a four-member dataset of the RCP8.5 scenario, each member differing in initial conditions. The area delimited by the two gray curves represents the range of model variability deduced from the four-member dataset.

water demand increases over the 21st century, due to the temperature increase. In average on the Sahel area, the water demand values rise from 580 mm (515 mm) to 650 mm (580 mm) per growing period for the sorghum (millet).

To quantify the impacts of rainfall decrease on the population, we analyze the gain or loss of available area for agriculture relative to the adequacy between the sorghum water requirement and the JJAS precipitation. Fig. 4A displays the variations of available area for sorghum cultivation. Under the GrIS scenarios, a strong decrease of the cultivable area with respect to 1976–2005 is observed between 2025 and 2100, up to $\sim 1,100,000 \text{ km}^2$ for the 1-m GrIS melting scenario and even more for the 1.5- and 3-m GrIS melting scenarios. After 2070, the cultivable area slightly increases, and the RCP8.5 values are progressively recovered, except for the 3-m scenario.

The large impact of the GrIS scenarios on the local population may be enhanced by a strong demography dynamics in the Sahel. All of the projections of the demography evolution suggest an increase of the population over Africa (40). However, these projections remain uncertain and are strongly dependent on socioeconomic changes that will occur throughout the 21st century (40, 41). To estimate the range of people affected by monsoon variations, we analyze the human impacts related to a loss of cultivable areas for a demography fixed to that of 2011 (lower bound) and for an evolving demography deduced from a shared socioeconomic pathway (41) (SSP3 hereafter), which is consistent with the RCP8.5 scenario (upper bound).

Considering the Sahelian population fixed to its 2011 level (i.e., 135 million people, Fig. 4B), the GrIS scenarios lead to a rapid growth (in less than 20 y) of people impacted by the loss of cultivable area, up to ~ 60 million people in the 1.5- and 3-m GrIS melting scenarios between 2040 and 2065, due to change in precipitation regimes. This number slightly decreases at the end of the FWF perturbation. However, the most dramatic consequences are observed when the population dynamics are accounted for (Fig. 4C). According to the SSP3 scenario, the number of people living below the water threshold (*Methods*) for sorghum cultivation undergoes a rapid and continuous increase, up to ~ 360 million by the end of the 21st century. This number represents one third of the population living in the Sahel area, showing that the climatic impact is widely amplified by the demography explosion. This situation will put a considerable strain on millet and sorghum subsistence agriculture. For local farmers, migration might thus appear as a necessary option, especially if one considers the rapid development of African metropolises. Options are, indeed, likely to be limited for local farmers, and staying on their land would require substantial changes in agricultural techniques and the abandonment of subsistence agriculture (42).

We demonstrated that Greenland melting during the 21st century could drastically affect the climate, not only in high-latitude locations but also over the tropical areas, through atmospheric and oceanic teleconnections. Although most studies focus on the coastal impacts of SLR (43), we pointed out that Greenland melting could produce drastic droughts in the Sahel, with many consequences for agricultural practices and for population migrations. In the past, monsoon-dependent farmers have used the cities (44) and the coastal zones as a refuge or a final migration destination following rainfall deficit years. Under the 1-m SLR scenario or one involving higher SLR, coastal zones will be extremely destabilized, and migration to these regions will be difficult, with a possible “coastal squeeze” (45), making the urban areas the primary destination for migrants. Today, most migrant flows related to environmental disruptions occur within their national or regional boundaries (46). A rapid melting of ice sheets, however, is likely to lead to dramatic population shifts that would develop beyond borders and would entail irreversible demographic impacts.

Methods

Model and Experimental Details. All of the experiments presented in this study have been carried out with the coupled atmosphere–ocean IPSL-CM5A-LR model (19), which has been used for the CMIP5 exercise. The atmospheric

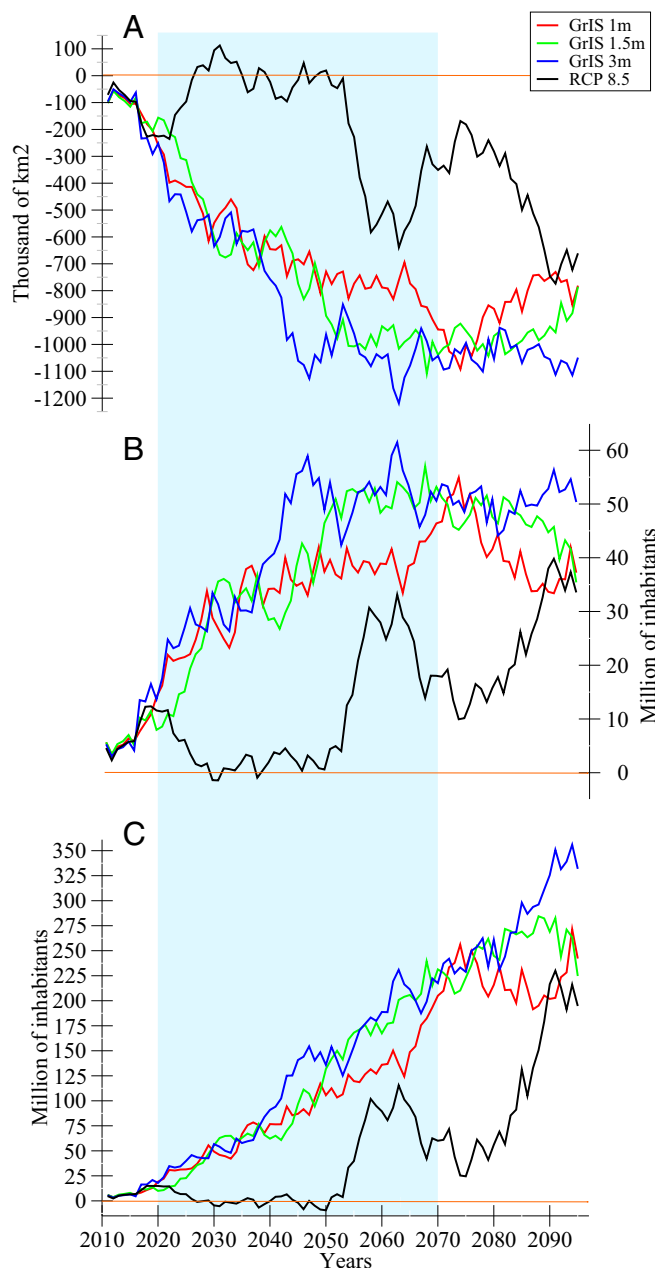


Fig. 4. Impacts of rainfall change on sorghum cultivation and on population. (A) Evolution of the surface area available for sorghum cultivation (i.e., when the average JJAS precipitation is above the sorghum water demand) for each GrIS scenario and for the baseline experiment. The evolution of the available cultivable area is given with respect to the available area averaged over the 1976–2005 reference period deduced from the historical IPSL-CM5A simulated precipitation. Negative (positive) values indicate a loss (gain) of cultivable area. (B) Evolution of the number of inhabitants living under the sorghum water demand with respect to the 1976–2005 historical reference period. This evolution is estimated with the assumption that the number of inhabitants is fixed to its 2011 level. (C) Evolution of the number of inhabitants living under the sorghum water demand with respect to the 1976–2005 historical reference period. Here, this evolution accounts for the evolution of demography provided by the SSP3 scenario. In both B and C, positive values indicate that the number of inhabitants living under the sorghum water demand increases with respect to the reference period.

component has a spatial resolution of $3.75^\circ \times 1.875^\circ$ in longitude and latitude, respectively, with 39 vertical levels; the oceanic component uses an irregular grid with a nominal resolution of 2° , and a higher latitudinal resolution of 0.5° in the equatorial ocean, and 31 vertical levels. The locations of

freshwater inputs have been designed to produce a rapid response of the model. We therefore chose to release the freshwater in locations of deep water formations, in the North Atlantic (45°N to 65°N , 45°W to 5°E), which also coincides with regions of input of Greenland meltwater (47). Recent papers pointed out relationships between Greenland melting and AMOC variations (48). The spread of FWF values (0.11 Sv to 0.68 Sv) has been chosen to explore the impact of a large and rapid freshwater input due to partial melting of the Greenland ice sheet. The highest FWF (0.68 Sv) accounts for the fact that current climate models are possibly too stable in response to freshwater release (49). A growing number of modeling results support this assumption by invoking (i) intrinsic model biases in advection (50–54) and/or in the stratification of the subpolar gyre (55), (ii) an incorrect representation of freshwater pathways in the absence of an iceberg drift module (10), or (iii) a too coarse resolution of current ocean models that are not eddy-resolving (56, 57). All these factors could potentially lead to a limited sensitivity of projected AMOC to freshwater input. Thus, we analyze here the progressive reduction of the AMOC corresponding to increased FWF and its potential impacts on the Sahelian region. More importantly, moderate scenarios (corresponding to 0.11 Sv to 0.34 Sv) have to be considered regarding the most recent ice sheet observations (e.g., refs. 13, 16, and 58).

Statistical Method to Adjust the IPSL Simulated Precipitation. The simulated precipitation has been corrected with respect to the WFDEI reanalyses interpolated to a $0.5^\circ \times 0.5^\circ$ spatial resolution (34), used as a reference. Here, the “calibration” period covers the 34-y time period 1979–2013, and the “projection” period covers the 94-y time period 2006–2099.

The bias correction method used in this study is a variant of the “Quantile Mapping” approach (e.g., refs. 59 and 60) and allows accounting for the climate change signal in the correction (37). This method, called CDF-t, was initially developed by ref. 61 and has since been applied in many climate-related studies (e.g., refs. 35–38, among others). If X denotes the random variable representing the modeled variable to be corrected, and Y is the random variable representing the reference variable, CDF-t first estimates the cumulative distributions F_{Yp} and F_{Xp} of the random variables Yp and Xp over the projection (future) time period before applying a distribution-derived quantile mapping, i.e., trying to map a modeled value x_p to a value y_p such that their distributions are equivalent (62),

$$F_{Yp}(y_p) = F_{Xp}(x_p) \Leftrightarrow y_p = F_{Yp}^{-1}[F_{Xp}(x_p)]. \quad [1]$$

If F_{Xp} can be directly modeled—parametrically or not—from the data to be corrected in the projection period, the modeling of F_{Yp} is based on the assumption that a mathematical transformation T allows going from F_{Xc} to F_{Yc} , the distribution of the random variables Yc and Xc in the calibration period,

$$T[F_{Xc}(z)] = F_{Yc}(z), \quad [2]$$

for any z , and that T is still valid in the projection period; that is,

$$T[F_{Xp}(z)] = F_{Yp}(z). \quad [3]$$

Replacing z by $F_{Xc}^{-1}(u)$ in Eq. 2, where u is any probability in $[0, 1]$, we obtain

$$T(u) = F_{Yc}[F_{Xc}^{-1}(u)], \quad [4]$$

corresponding to a simple definition for T . Inserting Eq. 4 in Eq. 3 leads to a modeling of F_{Yp} ,

$$F_{Yp}(z) = F_{Yc}[F_{Xc}^{-1}[F_{Xp}(z)]]. \quad [5]$$

Once F_{Xp} and then F_{Yp} are modeled, a distribution-based quantile mapping is applied as in Eq. 1. Hence, this CDF-t approach includes the information about the distributions over the projection time period in the quantile mapping technique. More details can be found in ref. 37.

To refine the bias correction method, a multivariate mapping could be performed, notably to better account for effect of the mesoscale processes [e.g., African easterly jet (AEJ) instabilities giving rise to squall lines] that could counteract those of the large-scale circulation. Such a multivariate approach would require wind data in altitude that are not currently available. Moreover, multivariate statistical bias correction methods are only emerging in the literature and are not yet ready to be used. However, paleoclimatic data reveal that ice sheet melting produced in the past a strong decrease of the West African monsoon (3–5) with underlying mechanisms fully similar to those highlighted in the present study (2), suggesting that the effect of jet instabilities is insufficient to counterbalance the effect of large-scale circulation (i.e., decrease of the monsoon rainfall).

t Test for Each Simulation. To investigate the significance of the monsoon variations due to the freshwater input, we use the *t* test. We average the total monsoon precipitation on the Sahel area (8°N to 18°N; 17°W to 15°E) and compare each scenario with the RCP8.5 baseline experiment. The *t* test (Eq. 6) must be done with stationary series,

$$t = \frac{\bar{X}_{scen} - \bar{X}_{rcp85}}{\sqrt{\frac{s_{scen}^2}{n_{scen}} + \frac{s_{rcp85}^2}{n_{rcp85}}}}, \quad [6]$$

where *t* is the *t* test result, *X* is the sample mean for the scenario under study and the RCP8.5 baseline scenarios, *S*² is the unbiased estimator of the variance of the two samples, and *n* is the simulated precipitation value in each scenario (i.e., 10 for the RCP8.5 baseline experiment and 10 for each GrIS scenario).

However, our scenarios are used in transient experiments. To circumvent this problem, we calculate the *t* test values 10 y by 10 y with a time lag of 1 y (i.e., 2006–2015, 2007–2016, ...) to obtain 84 pseudostationarity periods by subsampling. We obtain a *t* value for each year between 2011 and 2094. For each *t* test, we have 10 values for one GrIS scenario and 10 for the RCP8.5 one, leading to 18 degrees of freedom, allowing us to have a robust test. A longer period would lead to nonstationarity of our time series, and a shorter period would lead to a test with a too large variability, and therefore not usable. Using a probability threshold of 97.5% combined with these 18 degrees of freedom, the critical value is 2.101.

Water Demand of Crops. The threshold of crop water demand evolves with time as a function of temperature: The crops need more water when the temperature increases. The water demand of sorghum cultivation (ET_{crop}) can be obtained for each model grid point in the Sahel area (8°N to 18°N; 17°W to 15°E). It is estimated with the evapotranspiration (ET₀) given by the Blaney–Criddle technique (63) (Eq. 7) with a correction factor *kc*, as suggested by the FAO Eq. 8 (64), which accounts for specific characteristics of a given crop species,

$$ET_0 = p(0.46 T_{mean} + 8) \quad [7]$$

$$ET_{crop} = ET_0 \times kc \times A, \quad [8]$$

where ET₀ is the potential evapotranspiration (in millimeters per day), ET_{crop} is the water demand for crop (in millimeters per growing period), T_{mean} is the mean temperature over the monsoon period (in degrees Celsius), A is the crop growing period duration (i.e., 120 d for sorghum, 105 for millet), P is the percentage of daytime duration, and *kc* is the crop factor: 0.78 for sorghum, and 0.79 for millet.

Surface Area and Population Impacted by Rainfall Changes. To estimate the variations of the agricultural area due to rainfall changes and the number of inhabitants impacted by the weakening of precipitation, we computed the land surface area receiving an amount of precipitation below the required precipitation threshold for sorghum cultivations. Because the number of

inhabitants is given by a 0.5° × 0.5° spatial resolution dataset, provided by the Potsdam Institute for Climate Impact Research from a preliminary version of the SSP population data (the 2012-05-11 data in the International Institute for Applied Systems Analysis (IIASA) database), the rainfall has been bilinearly interpolated on a 0.5° × 0.5° grid. For each scenario (RCP8.5 and GrIS), the area impacted by rainfall change [R(t)] in the Sahel area (8°N to 18°N; 17°W to 15°E) is obtained year by year with the following equation:

$$R(t) = \sum R_{scen}(t) - \sum R_{ref}, \quad [9]$$

where R_{scen}(*t*) represents the area covered by the grid points where the precipitation volume is above the water demand of crops, and R_{ref} represents the area covered by the grid points where the precipitation averaged over the last 30-y climatic period (1976–2005) is above the water demand of crops.

To estimate the evolution of the cultivable area affected by a precipitation deficit, we express the number of corresponding pixels in square kilometers. When the number of pixels is negative (positive), the area available for agriculture is smaller (larger) than that of the 1976–2005 climatic period.

The number of inhabitants impacted by rainfall changes is estimated by summing the number of people living in the corresponding surface area. To count only the rural population with only rainfed agriculture practices, the surface area where the current population density is above 200 inhabitants per square kilometer is excluded. A positive (negative) value means that a greater (smaller) number of people is affected by rainfall changes compared with the reference period (1976–2005).

Code and Data Availability. All data generated in this study by the IPSL-CM5A-LR model for the Greenland scenarios as well as the Ferret and Python scripts produced for their analysis are available from the corresponding author. Other results supporting this study are based on CMIP5 model, WFDEI Reanalysis data, and population projections, which are available, respectively, from cmip5-pcmdi.llnl.gov/cmip5/data_portal.html, www.eu-watch.org/data_availability, and clima-dods.ictp.it/Users/fcolon_g/ISI-MIP/.

ACKNOWLEDGMENTS. We thank Michel Crucifix and an anonymous reviewer for their constructive comments and suggestions that helped improve the manuscript, as well as Serge Janicot and Juliette Mignot for fruitful discussions. We are also very grateful to Sarah Amram, Jean-Yves Peterschmitt, and Aurélien Quiquet for technical support, and to Sandra Bouneau and Sylvain David for numerous exchanges. This work was supported by the French Atomic Commission (CEA) within the framework of the Variations Abruptes du Climat: Conséquences et Impacts éNergétiques project funded by the Département des sciences de la matière (DSM) with the DSM-Energie Program. It benefited from the high performance computing (HPC) resources made available by Grand Equipement National de Calcul Intensif, CEA, and Centre National de la Recherche Scientifique. The authors thank the Potsdam Institute for Climate Impact Research for providing the gridded data population (SSP3) based on a preliminary version of the SSP population data (the 2012-05-11 data in the IIASA database). This database has been elaborated within the Inter-Sectoral Impact Model Intercomparison Project.

- Hulme M, Doherty R, Ngara T, New M, Lister D (2001) African climate change: 1900–2100. *Clim Res* 17:145–168.
- Mulitza S, et al. (2008) Sahel megadroughts triggered by glacial slowdowns of Atlantic meridional overturning. *Paleoceanography* 23:PA4206.
- Stager JC, Ryves DB, Chase BM, Pausata FSR (2011) Catastrophic drought in the Afro-Asian monsoon region during Heinrich event 1. *Science* 331:1299–1302.
- Itambi AC, Dobeneck T Von, Mulitza S, Bickert T, Heslop D (2009) Millennial-scale northwest African droughts related to Heinrich events and Dansgaard-Oeschger cycles: Evidence in marine sediments from offshore Senegal. *Paleoceanography* 24:PA1205.
- Tjallingii R, et al. (2008) Coherent high- and low-latitude control of the northwest African hydrological balance. *Nat Geosci* 1:670–675.
- Broecker W, Bond G, Klas M, Clark E, McManus J (1992) Origin of the northern Atlantic's Heinrich events. *Clim Dyn* 6:265–273.
- Alvarez-Solas J, Robinson A, Montoya M, Ritz C (2013) Iceberg discharges of the last glacial period driven by oceanic circulation changes. *Proc Natl Acad Sci USA* 110:16350–16354.
- Kageyama M, Mignot J (2009) Glacial climate sensitivity to different states of the Atlantic Meridional Overturning Circulation: Results from the IPSL model. *Clim Past* 5:551–570.
- Swingedouw D, et al. (2009) Impact of freshwater release in the North Atlantic under different climate conditions in an OAGCM. *J Clim* 22:6377–6403.
- Swingedouw D, et al. (2013) Decadal fingerprints of freshwater discharge around Greenland in a multi-model ensemble. *Clim Dyn* 41:695–720.
- Church JA, et al. (2013) Sea level change. *Climate Change 2013: The Physical Science Basis. Contribution of Working Group I to the Fifth Assessment Report of the Intergovernmental Panel on Climate Change* eds Stocker TF, et al. (Cambridge Univ Press, New York), pp 1137–1216.
- Straneo F, et al. (2013) Challenges to understanding the dynamic response of Greenland's marine terminating glaciers to oceanic and atmospheric forcing. *Bull Am Meteorol Soc* 94:1131–1144.
- Rignot E, Fenty I, Xu Y, Cai C, Kemp C (2015) Undercutting of marine-terminating glaciers in West Greenland. *Geophys Res Lett* 42:5909–5917.
- Gillet-Chaulet F, et al. (2012) Greenland ice sheet contribution to sea-level rise from a new-generation ice-sheet model. *Cryosphere* 6:1561–1576.
- Paolo FS, Fricker HA, Padman L (2015) Ice sheets. Volume loss from Antarctic ice shelves is accelerating. *Science* 348:327–331.
- Mouginot J, et al. (2015) Fast retreat of Zachariae Isstrøm, northeast Greenland. *Science* 350:1357–1361.
- Alvarez-Solas J, Ramstein G (2011) On the triggering mechanism of Heinrich events. *Proc Natl Acad Sci USA* 108:E1359–E1360.
- Gomez N, Gregoire LJ, Mitrovica JX, Payne AJ (2015) Laurentide-Cordilleran Ice Sheet saddle collapse as a contribution to meltwater pulse 1A. *Geophys Res Lett* 42:3954–3962.
- Dufresne J-L, et al. (2013) Climate change projections using the IPSL-CM5 Earth System Model: From CMIP3 to CMIP5. *Clim Dyn* 40:2123–2165.
- Manabe S, Stouffer RJ (1988) Two stable equilibria of a coupled ocean-atmosphere model. *J Clim* 1:841–866.
- Vellinga M, Wood RA, Gregory JM (2001) Processes governing the recovery of a perturbed thermohaline circulation in HadCM3. *J Clim* 15:764–780.
- Stouffer R, Yin J, Gregory J (2006) Investigating the causes of the response of the thermohaline circulation to past and future climate changes. *J Clim* 19:1365–1387.
- Kageyama M, et al. (2013) Climatic impacts of fresh water hosing under Last Glacial Maximum conditions: A multi-model study. *Clim Past* 9:935–953.
- Jackson R, et al. (2015) Global and European climate impacts of a slowdown of the AMOC in a high resolution GCM. *Clim Dyn* 45:1–18.

25. Swingedouw D, Braconnot P, Marti O (2006) Sensitivity of the Atlantic Meridional Overturning Circulation to the melting from northern glaciers in climate change experiments. *Geophys Res Lett* 33:L07711.
26. Peterson LC, Haug GH, Hughen KA, Röhl U (2007) Rapid changes in the hydrologic cycle of the tropical Atlantic during the last glacial. *Science* 290:1947–1951.
27. Leduc G, et al. (2007) Moisture transport across Central America as a positive feedback on abrupt climatic changes. *Nature* 445:908–911.
28. Chiang JCH, Bitz CM (2005) Influence of high latitude ice cover on the marine Intertropical Convergence Zone. *Clim Dyn* 25:477.
29. Arbuszewski JA, deMenocal PB, Cléroux C, Bradtmiller L, Mix A (2013) Meridional shifts of the Atlantic intertropical convergence zone since the Last Glacial Maximum. *Nat Geosci* 6:959–962.
30. Niedermeyer EM, et al. (2009) Extratropical forcing of Sahel aridity during Heinrich stadials. *Geophys Res Lett* 36:L20707.
31. Liu Y, Chiang JCH, Chou C, Patricola CM (2014) Atmospheric teleconnection mechanisms of extratropical North Atlantic SST influence on Sahel rainfall. *Clim Dyn* 43:2797–2811.
32. Ickowicz A, et al. (2012) Crop-livestock production systems in the Sahel - Increasing resilience for adaptation to climate change and preserving food security. *Building Resilience for Adaptation to Climate Change in the Agriculture Sector* (Food and Agric Org, Rome), pp 261–294.
33. Christensen JH, et al. (2013) Climate phenomena and their relevance for future regional climate change. *Climate Change 2013: The Physical Science Basis. Contribution of Working Group I to the Fifth Assessment Report of the Intergovernmental Panel on Climate Change*, eds Stocker TF, et al. (Cambridge Univ Press, New York), Chap 14.
34. Weedon GP, et al. (2014) The WFDEI meteorological forcing data set: WATCH Forcing Data methodology applied to ERA-Interim reanalysis data. *Water Resour Res* 50: 7505–7514.
35. Oettli P, Sultan B, Baron C, Vrac M (2011) Are regional climate models relevant for crop yield prediction in West Africa? *Environ Res Lett* 6:14008.
36. Colette A, Vautard R, Vrac M (2012) Regional climate downscaling with prior statistical correction of the global climate forcing. *Geophys Res Lett* 39:L13707.
37. Vrac M, et al. (2012) Dynamical and statistical downscaling of the French Mediterranean climate: Uncertainty assessment. *Nat Hazards Earth Syst Sci* 12:2769–2784.
38. Vignaud N, Vrac M, Caballero Y (2013) Probabilistic downscaling of GCM scenarios over southern India. *Int J Climatol* 33:1248–1263.
39. Sultan B, et al. (2013) Assessing climate change impacts on sorghum and millet yields in the Sudanian and Sahelian savannas of West Africa. *Environ Res Lett* 8:014040.
40. Kc S, Lutz W (2014) The human core of the shared socioeconomic pathways: Population scenarios by age, sex and level of education for all countries to 2100. *Global Environ Change* 42:181–192.
41. O'Neill BC, et al. (2014) A new scenario framework for climate change research: The concept of shared socioeconomic pathways. *Clim Change* 122:387–400.
42. Juana JS, Kahaka Z, Okurut FN (2013) Farmers' perceptions and adaptations to climate change in sub-Saharan Africa: A synthesis of empirical studies and implications for public policy in African agriculture. *J Agric Sci* 5:121–135.
43. Neumann B, Vafeidis AT, Zimmermann J, Nicholls RJ (2015) Future coastal population growth and exposure to sea-level rise and coastal flooding—A global assessment. *PLoS One* 10:e0118571.
44. Afolayan AA, Adelekan IO (1999) The role of climatic variations on migration and human health in Africa. *Environmentalist* 18:213–218.
45. Pontee N (2013) Defining coastal squeeze: A discussion. *Ocean Coast Manage* 84: 204–207.
46. McLeman RA, Hunter LM (2010) Migration in the context of vulnerability and adaptation to climate change: Insights from analogues. *Wiley Interdiscip Rev Clim Change* 1:450–461.
47. Bamber J, van den Broeke M, Ettema J, Lenaerts J, Rignot E (2012) Recent large increases in freshwater fluxes from Greenland into the North Atlantic. *Geophys Res Lett* 39:L19501.
48. Rahmstorf S, et al. (2015) Exceptional twentieth-century slowdown in Atlantic Ocean overturning circulation. *Nat Clim Change* 5:475–480.
49. Valdes P (2011) Built for stability. *Nat Geosci* 4:414–416.
50. Liu W, Liu Z, Brady EC (2014) Why is the AMOC monostable in coupled general circulation models? *J Clim* 27:2427–2443.
51. Liu W, Xie SP, Liu Z, Zhu J (2017) Overlooked possibility of a collapsed Atlantic Meridional Overturning Circulation in warming climate. *Sci Adv* 3:e1601666.
52. Deshayes J, et al. (2013) Oceanic hindcast simulations at high resolution suggest that the Atlantic MOC is bistable. *Geophys Res Lett* 40:3069–3073.
53. Hofmann M, Rahmstorf S (2009) On the stability of the Atlantic meridional overturning circulation. *Proc Natl Acad Sci USA* 106:20584–20589.
54. Weber SL, et al. (2006) The modern and glacial overturning circulation in the Atlantic Ocean in PMIP coupled model simulations. *Clim Past Discuss* 2:923–949.
55. Sgubin G, Swingedouw D, Drijfhout S, Mary Y, Bennabi A (2017) Abrupt cooling over the North Atlantic in modern climate models. *Nat Commun* 8:14375.
56. Spence P, Saenko OA, Sijp W, England MH (2013) North Atlantic climate response to Lake Agassiz drainage at coarse and ocean eddy-permitting resolutions. *J Clim* 26: 2651–2667.
57. Weijer W, Maltrud ME, Hecht MW, Dijkstra HA, Kliphuis MA (2012) Response of the Atlantic Ocean circulation to Greenland Ice Sheet melting in a strongly-eddy ocean model. *Geophys Res Lett* 39:L09606.
58. Noël B, et al. (2017) A tipping point in refreezing accelerates mass loss of Greenland's glaciers and ice caps. *Nat Comm* 8:14730.
59. Déqué M (2007) Frequency of precipitation and temperature extremes over France in an anthropogenic scenario: Model results and statistical correction according to observed values. *Global Planet Change* 57:16–26.
60. Gudmundsson L, Bremnes JB, Haugen JE, Engen-Skaugen T (2012) Technical Note: Downscaling RCM precipitation to the station scale using statistical transformations—A comparison of methods. *Hydrol Earth Syst Sci* 16:3383–3390.
61. Michelangeli P, Vrac M, Loukos H (2009) Probabilistic downscaling approaches: Application to wind cumulative distribution functions. *Geophys Res Lett* 36:L11708.
62. Panofsky HA, Brier GW (1958) *Some Applications of Statistics to Meteorology* (Pennsylvania State Univ, State College, PA).
63. Blaney HF, Criddle WD (1965) Determining water requirements for settling water disputes. *Nat Resour J* 4:29–41.
64. Food and Agriculture Organization (2016) Water Harvesting 2. Water and soil requirements. Available at www.fao.org/docrep/u3160e/u3160e04.htm. Accessed May 21, 2017.